

# Analyst

Accepted Manuscript



This is an *Accepted Manuscript*, which has been through the Royal Society of Chemistry peer review process and has been accepted for publication.

*Accepted Manuscripts* are published online shortly after acceptance, before technical editing, formatting and proof reading. Using this free service, authors can make their results available to the community, in citable form, before we publish the edited article. We will replace this *Accepted Manuscript* with the edited and formatted *Advance Article* as soon as it is available.

You can find more information about *Accepted Manuscripts* in the [Information for Authors](#).

Please note that technical editing may introduce minor changes to the text and/or graphics, which may alter content. The journal's standard [Terms & Conditions](#) and the [Ethical guidelines](#) still apply. In no event shall the Royal Society of Chemistry be held responsible for any errors or omissions in this *Accepted Manuscript* or any consequences arising from the use of any information it contains.

# Hyperspectral reflected light microscopy of plasmonic Au/Ag alloy nanoparticles incubated as multiplex chromatic biomarkers with cancer cells

Cite this: DOI: 10.1039/x0xx00000x

Received 00th January 2012,  
Accepted 00th January 2012

DOI: 10.1039/x0xx00000x

[www.rsc.org/](http://www.rsc.org/)

Sergiy Patskovsky, Eric Bergeron, David Rioux, Mikaël Simard and Michel Meunier.

École Polytechnique de Montréal, Laser Processing and Plasmonics Laboratory, Engineering Physics Department, Montréal, Québec, H3C 3A7, Canada. E-mail: [sergiy.patskovsky@polymtl.ca](mailto:sergiy.patskovsky@polymtl.ca)

A hyperspectral microscopy system based on a reflected light method for plasmonic nanoparticles (NPs) imaging was designed and compared with conventional darkfield method for spatial localization and spectroscopic identification of single Au, Ag and Au/Ag alloy NPs incubated with fixed human cancer cell preparations. New synthesis protocol based on co-reduction of Au and Ag salts combined with the seeded growth technique was used for the fabrication of monodispersed alloy NPs with sizes ranging from 30 to 100 nm in diameter. We validated theoretically and experimentally the performance of 60 nm Au, Ag and Au/Ag (50:50) NPs as multiplexed biological chromatic markers for biomedical diagnostics and optical biosensing. The advantages of the proposed reflected light microscopy method are presented for the NPs imaging in a complex and highly diffusing medium such as cellular environment. The obtained information is essential for the development of a high throughput, selective and efficient strategy for cancer detection and treatment.

## 1 Introduction

Recent years have seen tremendous progress in the design of regular nanoplasmonic structures and the synthesis of colloidal plasmonic nanoparticles (NPs) geared towards biological and biomedical applications. Indeed, the unique resonance properties of plasmonic NPs can be finely tuned by varying their size, shape, composition and mean inter-particle distance; therefore, they can be tailored for specific applications<sup>1</sup>. One notable example is the use of NPs as optical markers for biochemical and biomedical diagnostics, imaging of cells and tissues, detection and treatment of cancer cells<sup>2</sup>.

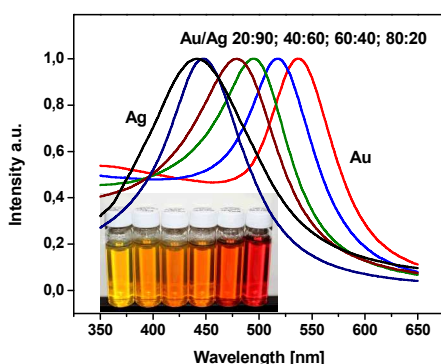
For many decades, combinations of fluorophores and antibodies have been used as biomarkers on cell surface. However, fluorophores typically show some limits, notably low sensitivity, difficult bioconjugation<sup>3</sup>, low quantum efficiency and a tendency to photobleach upon long exposure to the excitation light. With the advent of nanotechnology, quantum dots (QDs) have been considered as a promising alternative to replace conventional fluorophores<sup>4, 5</sup>. Among various QDs, CdSe and CdSe–ZnS are widely used in biology since their size-tunable photoluminescence distributed throughout the visible region of the electromagnetic spectrum make them good substitutes to organic dye molecules. Water-soluble and

bioconjugated CdSe–ZnS QDs offer new alternatives to organic dyes for cell labeling and imaging. However, the applications of QDs is limited by their blinking, a universally observed fluorescence intermittency which can be observed at the single nanocrystal level. These semiconductor nanocrystals (CdTe, CdSe, etc.) also raise potential toxicity issues since Cd atoms are toxic at very low concentration. Other major concerns in the applications of QDs are autofluorescence of tissues under visible light excitation, and the penetration depth of the excitation light and the emitted fluorescence light in tissues.

The higher photostability (non-photobleaching, non-photoblinking) of non-fluorescent plasmonic NPs is an interesting alternative to fluorescent molecules for real-time imaging of biomolecules. Noble metallic NPs, typically gold (Au) or silver (Ag), are widely used due to their plasmonic properties, photo-stability, water solubility and biocompatibility for *in vitro* and *in vivo* applications. The Au and Ag NPs are considered for cell labeling since they strongly scatter light and can be functionalized with different biomolecules via strong covalent binding between sulfur and the NP surface. Indeed, the scattering signal of a single plasmonic NP (60 nm diameter) is more than five orders of magnitude larger than the emission of a single fluorophore molecule. Thus, the detection sensitivity of these NPs should be in the subfemtomole range<sup>6</sup>. For a

1 multiplexed detection of various biomolecules on a biological  
 2 sample, several distinct probes should be used simultaneously.  
 3 The use of plasmonic Au/Ag alloy NPs with different  
 4 compositions and correspondingly different spectral signatures  
 5 functionalized with specific biomolecules fulfills this  
 6 requirement. However, reliable NPs visualization is assured by  
 7 sufficiently large NPs (>40 nm). Although the production of  
 8 suitably large pure Au or pure Ag NPs has been achieved for  
 9 many years, the synthesis of Au/Ag alloy NPs with  
 10 conventional methods generally results in NPs with a diameter  
 11 lower than 30 nm, which is too small for imaging  
 12 applications<sup>7,8</sup>.

13 In this article, we present and apply our new synthesis process  
 14 that satisfies the need for large, size-controlled and  
 15 monodispersed spherical plasmonic alloy NPs for scattering-  
 16 based imaging in a cellular environment. We experimentally  
 17 demonstrate the application of the individual Au, Ag and  
 18 Au/Ag NPs as multiplex chromatic biomarkers. We also built a  
 19 hyperspectral scanning microscopy system based on  
 20 conventional darkfield mode and reflected light mode for NPs  
 21 imaging. This method was used for spatial localization and  
 22 spectroscopic identification of Au, Ag and Au/Ag NPs  
 23 incubated as multiplex chromatic biomarkers with fixed human  
 24 cancer cell preparations in a cellular environment surrounded  
 25 with a physiological medium.



26  
27  
28  
29  
30  
31  
32  
33  
34  
35  
36  
37 **Fig. 1** Experimental spectra for different compositions of 60 nm Au/Ag  
 38 alloy NPs.

## 39 2 Experimental

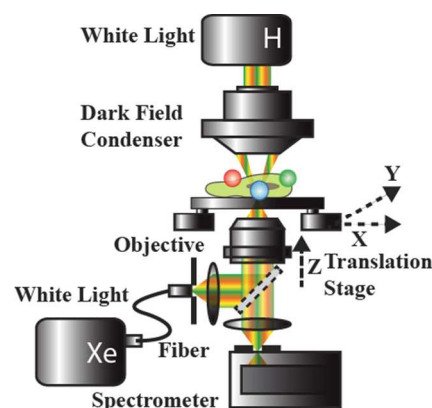
### 40 2.1 Synthesis of Au, Ag and Au/Ag alloy nanoparticles

41 Plasmonic NPs can be prepared by chemical<sup>7</sup> or laser ablation<sup>8</sup>  
 42 methods. However, these approaches are unable to fabricate  
 43 alloy NPs larger than 30 nm, setting certain limitations for the  
 44 wide application of the NPs as optical markers and bio-labels.  
 45 For this work, we developed a new synthesis protocol using a  
 46 combination of co-reduction of Au and/or Ag salts with a  
 47 seeded-growth technique for the fabrication of size-controlled  
 48 and monodispersed NPs. The seed NPs are Au NPs fabricated  
 49 by a standard Turkevich<sup>9</sup> approach, yielding NPs with a 13 nm  
 50 diameter. These NPs are then used as seeds for the growth of an  
 51 Au/Ag alloy by reduction of chloroauric acid (HAuCl<sub>4</sub>) and  
 52 silver nitrate (AgNO<sub>3</sub>) in a boiling aqueous solution of sodium  
 53 citrate. The composition of the alloy is controlled by the  
 54 relative amount of Au and Ag salts added. The final NP size is  
 55 controlled by the amount of metallic salt added to the initial  
 56 NPs seed. The method produces monodispersed spherical alloy  
 57 NPs with sizes from 30 to 100 nm in diameter and provides

58 precise control on the shape, composition and size of alloy NPs  
 59 during the synthesis. This method allows the synthesis of alloy  
 60 NPs with predictable and reproducible scattering spectrum that  
 could be biofunctionalized for cell imaging and targeting. Examples of the experimental spectra for different compositions of 60 nm alloy NPs are presented in Fig. 1. TEM measurements confirmed that the size distribution of the Au/Ag alloy NPs is narrow, with a coefficient of variation of 10%. It is expected that Au/Ag alloy NPs are not completely homogeneous in composition<sup>10</sup>. However, the impact of this effect on the spectral discrimination method will be minimal by using experimental reference spectra. The proposed technology is protected by a provisional patent<sup>11</sup> and a more detailed description of Au/Ag alloy NPs synthesis will be published soon.

### 61 2.2 Cell culture

62 MDA-MB-231 human breast cancer cells were cultured at 5000  
 63 cells/cm<sup>2</sup> in cell culture-treated polystyrene T75 flasks  
 64 (Sarstedt, Saint-Léonard, QC). Cells were grown in Dulbecco's  
 65 modified Eagle's medium (DMEM) containing 4.5 g/L D-  
 66 glucose, 584 mg/L L-Glutamine, 110 mg/L sodium pyruvate  
 67 and supplemented with antibiotics (100 units/mL penicillin and  
 68 100 µg/mL streptomycin, 1% PS) and 10% fetal bovine serum  
 69 (FBS, Life Technologies, Burlington, ON) in a humidified  
 70 incubator at 37°C under a 5% CO<sub>2</sub> atmosphere. Confluent cells  
 71 were removed by trypsinization and seeded onto glass bottom  
 72 dishes (1x10<sup>5</sup> cells, MatTek, Ashland, MA) for experiments in  
 73 DMEM supplemented with 1% PS and 10% FBS. When cells  
 74 reached 80% confluence, they were washed three times with  
 75 phosphate-buffered saline (PBS, Sigma-Aldrich), fixed with  
 76 ice-cold methanol at room temperature during 10 min and  
 77 washed three times with PBS. The petris were then kept at 4°C  
 78 until use. The cells were then incubated with NPs in PBS  
 79 during at least 1h at room temperature and observed by  
 80 microscopy.



81  
82  
83  
84  
85  
86  
87  
88  
89  
90  
91  
92  
93  
94  
95  
96  
97  
98  
99  
100  
**Fig. 2** Reflected light and darkfield hyperspectral microscopy set-up  
 using a 3D translation stage and an imaging spectrometer.

### 101 2.3 Hyperspectral microscopy

102 Hyperspectral imaging system for wide-field and spectral  
 103 examination of plasmonic NPs was built on the basis of an  
 104 inverted Eclipse Ti microscope (Nikon) equipped with a 100x  
 105 oil immersion objective (numerical aperture (NA) = 0.5-1.3,  
 106 Nikon) (Fig. 2). The output microscopic image was aligned  
 107 with the input slit on an imaging spectrograph (Shamrock 750,  
 108 Andor Technology) equipped with an EMCCD detecting

camera (Newton 971, 1600x400 pixels, Andor Technology) and a 150 lines/mm grating providing 242 nm bandpass. A flat top inverted microscope motorized stage (ProScan, Prior Scientific Inc., Rockland, MA) allows fine three-dimensional (3D) spatial sample translation. To obtain hyperspectral data cube for further 2D spectral analysis, the stage acts as a "push broom", moving the sample precisely over the hyperspectral image detector<sup>12</sup>. This optical set-up was designed to provide two complementary modes of hyperspectral sample evaluation. The first method uses microscopy with conventional darkfield illumination (darkfield condenser from Nikon, NA = 0.95-0.80) forming hyperspectral imaging by transmitted light similar to commercial devices (CytoViva, Auburn, AL; PARISS, LightForm Inc., Asheville, NC). In this configuration, a standard white light source (Nikon) with 50 W halogen lamp provided a smooth illumination spectrum in the operating range from 400 to 630 nm. The second microscopy configuration was designed specifically for this project and worked on the principle of reflected light hyperspectral microscopy. Reflected light mode requires high level of light illumination collimation that was provided here by a Xenon light source (Newport, Irvine, CA) coupled to a liquid optical fiber and reflected from a 90:10 beam splitter (Thorlabs, Newton, NJ) (Fig. 2). The characteristic spectral ripples of the Xenon light in the UV range were subtracted by the acquisition software. Custom-written LabView software controlled the motorized stage displacements to synchronize sample movements with spectral image acquisition (National Instruments, Austin, TX). This software was also used for further analysis of the obtained hyperspectral data cube.

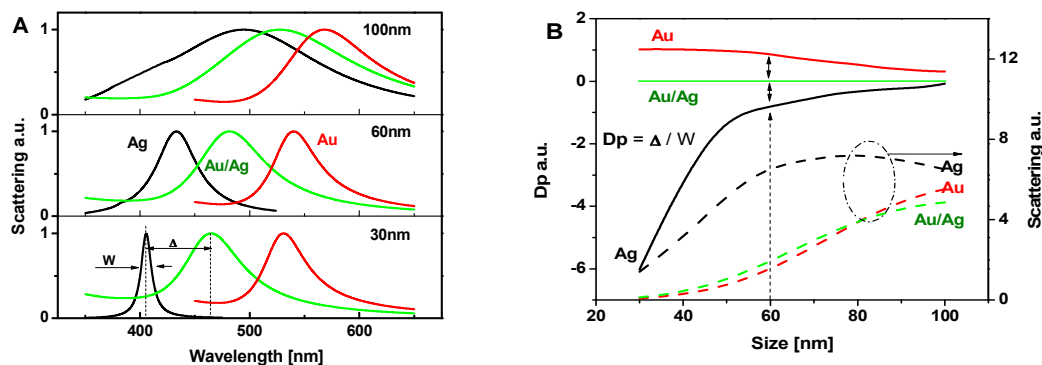


**Fig. 3** A) Normalized theoretical scattering spectra of 30, 60 and 100 nm diameter Au, Ag and Au/Ag (50:50) NPs. B) Discrimination parameter ( $D_p$ ) and scattering efficiency dependence with NP diameters.

We introduced here a simplified discrimination parameter  $D_p$  defined by the ratio of the difference between the biomarker and the reference resonance peak wavelengths ( $\Delta$ ) on the full width at half maximum of the biomarker spectral characteristic ( $W$ ) (Fig. 3A,B). As a reference point, we used the spectral position of the resonance peak for Au/Ag (50:50) NPs. Calculations show that smaller NPs lead to an increase in  $\Delta$  and a decrease in  $W$ , thus resulting in an increase of the discrimination parameter  $D_p$ . For example, for 30 nm NPs calculated by Mie theory, the parameter  $\Delta = 406$  nm (Ag) – 476 nm (Au/Ag) = -70 nm,  $W(\text{Ag}) = 11.6$  nm and corresponding  $D_p = \Delta/W = -6.03$  (Fig. 3B). Larger NPs facilitate optical detection due to higher scattering efficiency, whereas smaller NPs provide better spectral discrimination (Fig. 3B). A similar trend is observed for the corrected parameter  $D_p$  calculated for NPs

### 3 Results and discussion

#### 3.1 Characterization of Au, Ag and Au/Ag nanoparticles as biosensing markers with spectral discrimination

Application efficiency of colloidal plasmonic NPs with different spectral signature as chromatic biomarkers depends directly on the NPs plasmonic characteristics described by the corresponding resonance extinction and scattering spectra. The Au/Ag alloy NPs can be considered as good candidates for multiple chromatic biomarkers with spectral discrimination, as they offer several advantages, namely a fine spectral tuning of scattering spectra, sufficiently narrow spectral peaks and appropriate physicochemical properties for surface biofunctionalization.

Theoretical scattering spectra of Au, Ag and Au/Ag NPs with different diameters in liquid medium were computed using Mie Theory. The corresponding dielectric functions for the plasmonic alloy NPs were calculated using an analytical model based on the spectroscopic ellipsometry measurements of the dielectric functions of thin Au/Ag films<sup>13</sup>. Figure 3A shows the theoretical spectra for the normalized scattering cross section of 30, 60 and 100 nm NPs with three different compositions: pure Au, pure Ag and Au/Ag (50:50). For these NPs compositions, the peak redshifts, broadens, and intensifies with an increase in NP size (Fig. 3). By increasing the NP size, the differences between the positions of the scattering maxima decrease and the width of the plasmon peak becomes broader, thus indicating that spectral discrimination should become more difficult for larger NPs.

in a higher refractive index (RI) medium such as a cellular environment.

As a conclusion, for reliable hyperspectral imaging with conventional darkfield illumination and multiple NPs spectral markers, the optimal relation between the NPs scattering intensity and spectral signature has to be determined. Considering the results presented in Fig. 3 and the results published in the literature<sup>14</sup>, 60 nm NPs were chosen for the following experiments.

#### 3.2 Hyperspectral imaging of nanoparticles

Spectral characterization and discrimination of plasmonic NPs as biological markers usually imply measurements of extinction-scattering spectra in the range of the characteristic plasmon resonance peak. Depending on the application, such

measurements can be performed on the entire array of NPs<sup>15</sup> with consecutive numerical treatment of the single output spectrum with several peaks. This method is simple, but lacks discrimination precision. A more sophisticated and sensitive method is hyperspectral imaging, where the complete resonance characteristics and the spatial distribution of each individual NP can be obtained and analyzed.

When plasmonic NPs are designed as biomarkers for multi-sensing of analytes (DNA, proteins, antigens), the surrounding medium is usually optically homogeneous. In this case, hyperspectral microscopy based on the conventional darkfield mode performs well for chromatic plasmonic NP imaging (section 3.2.1). Optical detection of biomarkers used for imaging of cells and tissues is more complicated as highly diffusing and dynamically instable cellular medium drastically increases background noise. To solve this problem, we developed a hyperspectral set-up based on the reflected light mode to detect NPs in a cellular environment for which promising experimental results are obtained and presented in section 3.2.2.

### 3.2.1 Hyperspectral darkfield microscopy

Experimental evaluation of the plasmonic NPs with different compositions and diameters at the single-particle level in water, a uniform low diffusing medium, was performed in a hyperspectral darkfield microscopy configuration (Fig. 2). As expected, large single NPs (>100 nm) were easily detected and spectrally identified. The limit of detection for our optical set-up was estimated at about 50 nm in water. As an example, in Fig. 4A, the darkfield image captured by a color camera is presented for the three plasmonic 60 nm NP markers: Au, Ag and Au/Ag NPs. The sample preparation includes similar NP concentrations in deionized water and physical adsorption during at least one hour on the glass bottom petri dish surface in the absence of cells. A 100x oil immersion objective (NA = 0.7) was used for the NPs visualization with an available additional 1.5x magnification. Small field aperture for the illumination source and double annular slit in the darkfield condenser was used to improve light collimation and image contrast.

Experimental hyperspectral scan was performed with 200 nm displacement step, 3s time constant for each spatial line and 100  $\mu\text{m}$  spectrometer slit. A 2D CCD camera of the imaging spectrometer (Fig. 2) provides spatial information on one axis whereas the other axis is assigned to the wavelength. A scattering spectrum from one NP is extracted by integrating the intensity in spatial direction where the selected NP is identified. The background spectrum is taken from the surrounding environment without NPs and then subtracted from the NPs spectrum<sup>16</sup>. A reconstructed intensity image, shown in Fig. 4B, is obtained by integrating the spectrum of each pixel of the spatial image. The positions of single NPs are obtained in area where the detected scattering intensity is three times higher than the background noise and verified by comparing the experimental spectra to the theoretical ones. The experimental NPs spectra were normalized to facilitate comparison with theoretical results from Mie Theory and subsequent spectral discrimination. The results are presented in Fig. 4C and exhibit certain variations of the spectral peak position from one NP to the other. NP size distribution, adjacent substrate, spatial drift of the sample and mechanical stability of the system could induce such variations. It should be noted that the Ag NPs are almost twice more sensitive to changes in the medium RI, thus resulting in greater variations of the experimental spectra. Color

rendering of hyperspectral image provides information for preliminary visual NPs localization and spectral discrimination. This color reconstruction was performed by using standard sensitivity functions from the International Commission on Illumination (CIE)<sup>17</sup> and reconstructed color image is shown in Fig. 4D. Each NP composition is easily visualized by a specific color (Fig. 4A, Blue: AgNP, Green: Au/Ag NP, Yellow: AuNP) and the corresponding hyperspectral scan after color rendering of spectra for each pixel provides similar spatial and color image (Fig. 4D).

Thus, synthesis of large alloy NPs used as chromatic markers in a uniform low diffusing medium could simplify spectral classification. Expensive hyperspectral scanning system in this case can be replaced by a conventional RGB color camera. From obtained experimental results and theoretical calculations, we can estimate that up to five 60 nm Au/Ag NPs in different alloy compositions could be used for the chromatic labeling in optical biosensing. Application of more sophisticated numerical treatment for the experimental hyperspectral data using linear spectral unmixing method and spectral angle mapper could greatly improve system resolution and would be absolutely necessary for commercial devices. Smaller NPs could be detected to provide higher spectral discrimination. However, in this article, we want to demonstrate the working principle using conventional microscopy set-up where reliable single NP visualization and spectral discrimination is obtained with 60 nm NPs, which we consider as the optimal size in a uniform low diffusing medium.

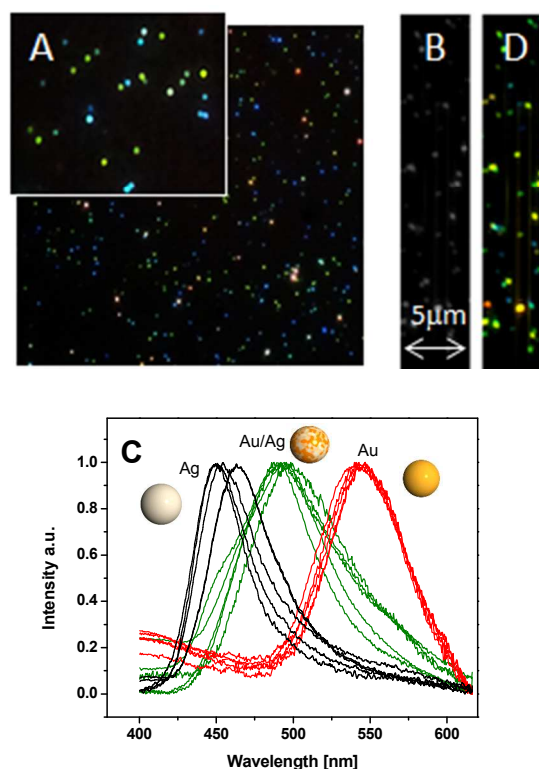


**Fig. 4** Experimental results for three compositions of 60 nm NPs: Au, Ag and Au/Ag (50:50). A) Darkfield microscopy color image. B) Intensity and D) color image numerically reconstructed from hyperspectral data obtained by hyperspectral 2D scan performed with 100x oil immersion objective, 200 nm displacement step, 3s time constant and 100  $\mu\text{m}$  spectrometer slit. C) Normalized experimental NPs spectra.

### 3.2.2 Hyperspectral reflected light microscopy of NPs incubated with cells

Information about NPs concentration, spatial 3D localization and spectral characteristics of single and aggregated NPs is very important for selective detection of cells labeled with NP markers in biochemical or biomedical applications. Here, we investigated the efficiency of chromatic labeling of cancer cells with Au, Ag and Au/Ag NPs in a physiological medium. For these experiments, fixed MDA-MB-231 cells were incubated with the NPs during at least 1h. At this step, the cells were visualized by conventional darkfield microscopy. Large NPs (>100 nm) were readily detected and easily identified. Next experiments were performed with 60 nm Au, Ag and Au/Ag NPs to estimate the efficiency of visualization and chromatic discrimination with our experimental set-up. The influence of cellular environment on the quality of NPs optical detection was clearly visible in darkfield imaging of cancer cells incubated with the NPs (Fig. 5A). Image interpretation and NP imaging was quite complicated or even impossible since intense light scattering from the cells completely covered the light scattered from 60 nm NPs. Therefore, the direct application of

60 nm NPs in a conventional darkfield illumination transmitted microscopy could not be recommended for cells-NPs complex imaging. Since 60 nm and smaller NPs provide higher potential for biomarkers with spectral discrimination, a more efficient NPs imaging set-up should be developed.

In this article, we propose a hyperspectral optical arrangement based on a reflected light method for plasmonic NPs imaging realized on the same inverted Eclipse Ti microscope used for conventional darkfield imaging (Fig. 2). Experimental results using reflected light microscopy revealed drastic improvements in the visualization of plasmonic NPs in a cellular environment in comparison to conventional darkfield microscopy (Fig. 5). Imaging with 100x oil immersion objective with NA = 1.3 provided excellent contrast for NP spatial distribution and thus facilitate spectral characterization in the area covered with or without cells. In Fig. 5A1-C1, we show examples of the 3D intensity pattern of the point-spread function for NPs on the cellular background that confirms advantages of the proposed method. Moreover, scanning in the z-direction resulted in the detection of NPs on cells at different distances from the glass substrate (Fig. 5B-C, Video<sup>18</sup>).

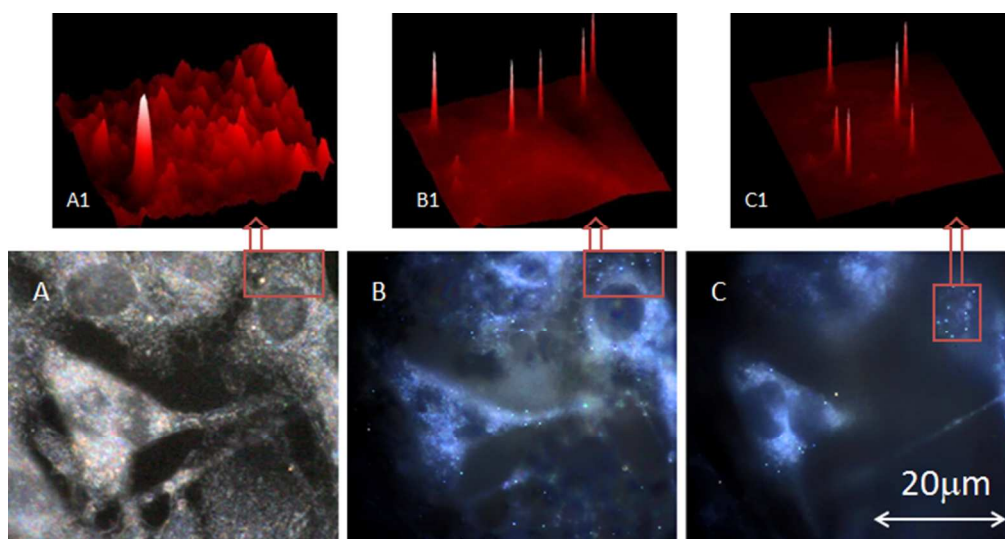


**Fig. 5** A) Darkfield imaging of fixed MDA-MB-231 cells incubated with Au, Ag and Au/Ag NPs during at least 1h. B, C) Backscattering images of the same area were taken at different planes along the optical z axis. All images were taken with 100x oil immersion objective. A1, B1, C1) Corresponding 3D intensity pattern of the point-spread function for NPs on the cellular background.

The proposed imaging method is based on a reflected light microscopy mode adapted for NPs visualization, where NPs contrast is improved by the following three approaches. First, an immersion objective was used to minimize backreflected light from the substrate (Fig. 6). An additional antireflection coating between glass substrate and liquid medium could also help to eliminate or reduce backreflection from this interface, thus improving NPs contrast. Second, high NA objectives are used. Intrinsic limitation of darkfield microscopy about the objective NA ( $NA_{\text{objective}} < NA_{\text{condenser}}$ ) is removed, thus resulting in high contrast imaging of NPs and precise 3D NPs spatial localization. Third, backscattering mode is applied for cells-NPs complex imaging<sup>19</sup>. In conventional transmission darkfield illumination, the contrast between the NPs and the cells is generally low because the cells have a strong forward scattering signal. Since the cells generally have a much lower backscattering signal and NPs have a similar front and

backscattering signal, it is advantageous to consider backscattering imaging in order to achieve better contrast of the NPs over the cells. Commercial epi-illumination darkfield objectives designed for surface analysis are incompatible with index-matching fluids, have limited numerical aperture and are still rather expensive.

The proposed reflected light technology is protected by a provisional patent<sup>20</sup> and could be used as an alternative to confocal microscopy<sup>21</sup> for fast 3D wide-field scanning of cells labeled with 60 nm plasmonic NPs. However, to obtain complete cellular images, the application of numerical imaging method is needed to reconstruct wide-field image from multiple z-scans.

An interesting phenomenon was observed when the microscope focal point was located on the plane with NPs on the glass-liquid interface. The image background was partially formed by the light reflected from the backside of the microscope slides,

usually about 0.12–0.17 mm thick (Fig. 6). Experimental spectra of Au/Ag NPs obtained at four different NA with an adjustable NA 100x oil immersion objective was gradually transformed from pure absorption behavior at NA = 0.5 to backscattering NPs response at NA = 1.3. Correspondingly, dark or bright spots were detected on the images taken by objective with low or high NA, respectively (Fig. 6B). These results show that spectral characterization of NPs in a cellular environment attached or close to the substrate can be rather complicated since the spectral interpretation involves not only the size of NPs but also the optical collection angle (solid angle). We observed no similar effects for the NPs located at increasing distance from the glass substrate, so we assume that this effect is mainly the result of interferometry with normally reflected light from the glass substrate/liquid medium interface<sup>22</sup>.

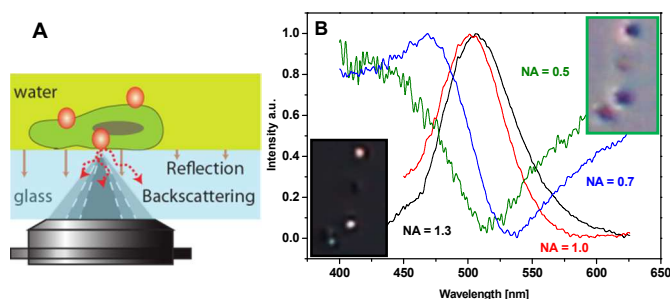


**Fig. 6** A) Optical configuration for hyperspectral backscattering analysis of NPs. B) Spectral characteristics of Au/Ag (50:50) NPs with an adjustable NA 100x oil immersion objective.

Hyperspectral scan of the cells-NPs complex was performed in reflected light optical configuration with 100x immersion objective (NA = 1.3) at a fixed focal plane in the z-direction, 200 nm displacement step of the translation stage, 1s time constant and 100  $\mu$ m spectrometer slit. The intensity image reconstructed from hyperspectral scan data is shown in Fig. 7A. For better clarity, an embossing filter was applied to the image. Examples of spatial positions of Au, Ag and Au/Ag NPs are shown on the image (Fig. 7B). The presence of NPs was detected by analyzing the local point-spread function intensity. The corresponding local spectrum was found by removing the background taken from 20 pixel radius annular region at 20 pixel distance. Then, NPs compositions were confirmed by comparing experimental and theoretical spectra of single NPs (Fig. 7C). The hyperspectral system with proposed reflected light optical mode allows the chromatic visualization and discrimination of 60 nm plasmonic NPs made of different compositions, thus providing new multiplexing opportunities for bioapplications. The proposed method is especially advantageous for the NPs imaging in a complex highly diffusing medium (Fig. 5B-C, Video<sup>18</sup>). These plasmonic NPs will be functionalized with different biomolecules such as DNA or antibodies to selective target specific biomarkers such as antigens or proteins. Indeed, the visualization of these NPs should provide an interesting way to characterize single and aggregated NPs in a biological context. Epi-illumination mode also provides unrestricted access to the sample and could be easily combined with traditional fluorescence imaging approach.

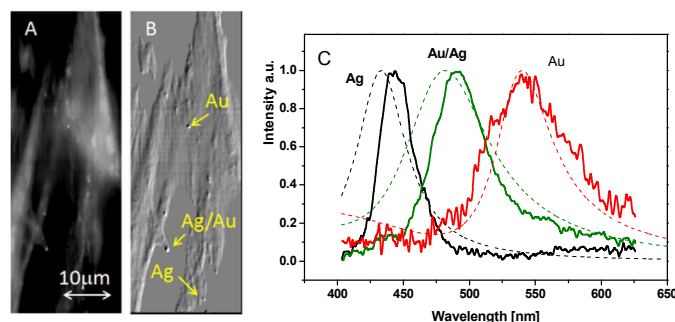


**Fig. 7** A) A reconstructed intensity image obtained by hyperspectral scanning in reflected light optical configuration. Scan was performed with 100x oil immersion objective, 200 nm displacement step, 1s time constant and 100  $\mu$ m spectrometer slit. B) For better clarity an embossing filter was applied to show the positions of Au, Ag, Au/Ag (50:50) NPs. C) The corresponding experimental and theoretical NPs spectra are presented by solid and dashed lines, respectively.

## 4 Conclusion

We propose and experimentally demonstrate the application of 60 nm plasmonic Au/Ag alloy NPs fabricated by a proprietary synthesis method as biosensing and imaging markers in a biological medium. Two biological application avenues were considered involving different complexity of tested media and detection optical set-ups. The hyperspectral imaging system with a reflected light microscopy mode is suitable for NPs imaging in a highly diffusing medium. We expect that this setup in combination with Au/Ag NP biomarkers will find wide applications in various fields of chemical identification and biomedical diagnosis and treatment where spatial and spectral analyses of NPs are essential. Presented system capability for 3D NP tracking will also enable investigation of specific cellular activity with the use of NPs as spectral sensors.

## 5 Acknowledgements

The authors thank Le Fonds de recherche du Québec – Nature et technologies and Le Fonds de recherche du Québec – Santé for the financial support.

## Notes and references

1. K. A. Willets and R. P. Van Duyne, *Annu Rev Phys Chem*, 2007, 58, 267-297.
2. X. H. Huang, P. K. Jain, I. H. El-Sayed and M. A. El-Sayed, *Nanomedicine-Uk*, 2007, 2, 681-693.
3. W. Sigmund, H. El-Shall, D. O. Shah and B. M. Moudgil, *Particulate Systems in Nano- and Biotechnologies*, CRC Press 2008.
4. M. Y. Han, X. H. Gao, J. Z. Su and S. Nie, *Nat Biotechnol*, 2001, 19, 631-635.
5. X. H. Gao, Y. Y. Cui, R. M. Levenson, L. W. K. Chung and S. M. Nie, *Nat Biotechnol*, 2004, 22, 969-976.
6. A. Taylor, K. M. Wilson, P. Murray, D. G. Fernig and R. Levy, *Chem Soc Rev*, 2012, 41, 2707-2717.
7. S. Link, Z. L. Wang and M. A. El-Sayed, *J Phys Chem B*, 1999, 103, 3529-3533.
8. S. Besner and M. Meunier, *J Phys Chem C*, 2010, 114, 10403-10409.
9. J. Turkevich, P. C. Stevenson and J. Hillier, *Discuss. Faraday Soc*, 1951, 11.

## Journal Name

10. D. Mahl, J. Diendorf, S. Ristig, C. Greulich, Z. A. Li, M. Farle, M. Koller and M. Epple, *J Nanopart Res*, 2012, 14.
11. D. Rioux and M. Meunier, *USPTO61945276*, 2014.
12. A. R. Badireddy, M. R. Wiesner and J. Liu, *Environmental Science & Technology*, 2012, 46, 10081-10088.
13. D. Rioux, S. Vallieres, S. Besner, P. Munoz, E. Mazur and M. Meunier, *Adv Opt Mater*, 2014, 2, 176-182.
14. P. K. Jain, K. S. Lee, I. H. El-Sayed and M. A. El-Sayed, *J Phys Chem B*, 2006, 110, 7238-7248.
15. K. Seekell, M. J. Crow, S. Marinakos, J. Ostrander, A. Chilkoti and A. Wax, *J Biomed Opt*, 2011, 16.
16. S. Takumi, J. Junesch and P. Rajendran, in *Optical Imaging: Technology, Methods and Applications*, eds. A. Tanaka and B. Nakamura, Nova Science Publishers, 2012.
17. F. W. Billmeyer and M. Saltzman, *Principles of color technology*, Interscience Publishers ;, New York, 1966.
18. Nanoparticles imaging.  
"http://www.groupes.polymtl.ca/lpl/?q=en/projet/nanoparticles-imaging"
19. S. Patskovsky, E. Bergeron and M. Meunier, *Journal of biophotonics*, 2013, DOI: 10.1002/jbio.201300165.
20. S. Patskovsky, D. Rioux, M. Meunier and É. Bergeron, *05015490-95USPR*, 2014.
21. S. Klein, S. Petersen, U. Taylor, D. Rath and S. Barcikowski, *Journal of Biomedical Optics*, 2010, 15.
22. K. Lindfors, T. Kalkbrenner, P. Stoller and V. Sandoghdar, *Physical Review Letters*, 2004, 93.